Pharm Res (2015) 32:1325–1340
DOI 10.1007/s11095-014-1537-6

RESEARCH PAPER

# Reduction-responsive Crosslinked Micellar Nanoassemblies for Tumor-targeted Drug Delivery

Wei Fan • Yingzhe Wang • Xin Dai • Lei Shi • DeAngelo Mckinley • Chalet Tan

Received: 9 June 2014 / Accepted: 29 September 2014 / Published online: 16 October 2014


## ABSTRACT

***Purpose*** The purpose of the study was to devise and evaluate crosslinked nanoassemblies to achieve enhanced drug delivery to tumors.

***Methods*** A novel copolymer comprised of polyethylene glycol 5000 ($PEG_{114}$), Vitamin E (VE) and thioctic acid (TA) with a molar ratio of $PEG_{114}$:VE:TA at 1:4:4 was synthesized. The resulting $PEG_{114}$-$VE_4$-$TA_4$ copolymer self-assembled into micelles, which formed polydisulfide crosslinks catalyzed by dithiothreitol. Employing paclitaxel as a model drug, the crosslinked $PEG_{114}$-$VE_4$-$TA_4$ micelles were characterized for the physicochemical and biological properties. The pharmacokinetics and anticancer efficacy of paclitaxel-loaded crosslinked $PEG_{114}$-$VE_4$-$TA_4$ micelles were assessed in a human ovarian cancer xenograft murine model.

***Results*** The crosslinked $PEG_{114}$-$VE_4$-$TA_4$ micelles demonstrated markedly improved thermodynamic and kinetic stability. The disulfide crosslinks were responsive to the intracellular level of glutathione, which caused rapid disassembly of the micelles and accelerated drug release. Intravenous administration of paclitaxel-loaded crosslinked $PEG_{114}$-$VE_4$-$TA_4$ micelles yielded approximately 3-fold and 5-fold higher plasma concentration than the non-crosslinked micelles and Taxol®, respectively, leading to increased drug accumulation in the tumor. Importantly, paclitaxel-loaded crosslinked micelles exerted superior tumor growth repression compared to the non-crosslinked counterparts and Taxol®.

***Conclusions*** These results suggest that the crosslinked $PEG_{114}$-$VE_4$-$TA_4$ nanocarrier system is a promising platform for the delivery of hydrophobic anticancer agents.

**KEY WORDS** crosslinked micelles · disulfide crosslinks · nanocarriers · paclitaxel · pharmacokinetics

## ABBREVIATIONS

| | |
|---|---|
| B-CMs | Blank crosslinked micelles |
| B-NCMs | Blank non-crosslinked micelles |
| CMC | Critical micelle concentration |
| DiD | 1,10-dioctadecyl-3,3,30,30-tetramethylindodicarbocyanine perchlorate |
| DiI | 1,1'-dioctadecyl-3,3,3',3'-tetramethylindocarbocyanine perchlorate |
| DiO | 3,3'-dioctadecyloxacarbocyanine perchlorate |
| DLS | Dynamic light scattering |
| DP-CMs | DiD/paclitaxel-dual loaded crosslinked micelles |
| DP-NCMs | DiD/paclitaxel-dual loaded non-crosslinked micelles |
| DTT | Dithiothreitol |
| EPR | Enhanced permeability and retention |
| FRET | Fluorescence energy transfer |
| GSH | Glutathione |
| H&E | Hematoxylin and eosin |
| NIR | Near Infrared |
| P-CMs | Paclitaxel-loaded crosslinked micelles |
| PCNA | Proliferating cell nuclear antigen |
| P-NCMs | Paclitaxel-loaded non-crosslinked micelles |
| SDS | Sodium dodecyl sulfate |
| TA | Thioctic acid |
| TEM | Transmission electron microscopy |

**Electronic supplementary material** The online version of this article (doi:10.1007/s11095-014-1537-6) contains supplementary material, which is available to authorized users.

W. Fan • Y. Wang • X. Dai • D. Mckinley • C. Tan (✉)
Cancer Nanomedicine Laboratory Department of Pharmaceutical Sciences, Mercer University College of Pharmacy, 3001 Mercer University Drive, Atlanta, Georgia 30341, USA
e-mail: tan_c@mercer.edu

L. Shi
School of Life Sciences, Nanjing University, 22 Hankou Road, Nanjing, Jiangsu 210093, China

VE Vitamin E

## INTRODUCTION

Polymeric micelles are versatile drug carrier systems that demonstrate great promise in the delivery of anticancer drugs. Currently there are six micellar formulations undergoing clinical trials and many more being explored in the preclinical studies (1). Composed of diverse amphiphilic copolymers, polymeric micelles are self-assembled supramolecular aggregates displaying typical core-shell architecture. While polyethylene glycol (PEG) is the most commonly employed hydrophilic block which shields the nanoconstructs and confers the stealth property by sterically hindering protein adsorption, the chemical structure of the hydrophobic segment can be tailored to optimize the encapsulation of the payload (2). Indeed, one major advantage of the micellar nanocarriers is their tunable loading capacity for the hydrophobic drugs within the highly lipophilic micellar core *via* physical entrapment, which alleviates the use of organic solvents and greatly increases the aqueous solubility of otherwise water-insoluble drugs (3).

Another potential advantage of polymeric micelles for cancer therapy resides in their nanoscale dimensions, which can allow for passive targeting of anticancer drugs to the tumor *via* the enhanced permeability and retention (EPR) effect owing to the leaky vasculature and diminished lymphatic drainage in solid tumors (4). To realize this benefit, it is imperative that the micelles maintain structural integrity and retain the payload for sufficient duration while circulating in the bloodstream. However, thermodynamic and kinetic instability of the micelles *in vivo* poses significant challenges for minimizing the burst release of the payload prior to the arrival of the drug-loaded micelles at the tumor site (5). As self-assembled aggregates, micelles undergo dynamic equilibrium with the constituting polymeric unimers. In the circulation, continuous removal of the unimers *via* metabolism and/or renal excretion shifts the equilibrium toward structural disintegration of the micelles. Moreover, binding of polymers to the plasma proteins and the cellular components in blood further destabilize the micelles, resulting in rapid dissociation of the drug molecules from the micelles (6).

To reinforce structural integrity of polymeric micelles and assist these nanoassemblies in withstanding the destabilizing environment *in vivo*, one promising approach is to covalently crosslink adjacent polymeric chains in the micelle to generate a single, nanostructured macromolecule. Various chemical reactions, such as radical polymerization, UV crosslinking, disulfide linkage, polyelectrolyte complexation, silicon chemistry and click chemistry, have been explored to devise the crosslinked micelles (7–10). By conjugating the polymer backbone with cross-linkable moieties or introducing external bifunctional crosslinkers, cross-linkages may be formed at the shell, core or core-shell intermediate region of the micelles. For the crosslinked micelles to serve as biocompatible and biodegradable drug carriers, it is important that the crosslinking reactions occur in aqueous solution, employ/produce non-toxic substances, and are readily reversible in the tumor to facilitate the release of the payload and the elimination of the polymers.

Disulfide linkage represents an appealing crosslinking strategy that demonstrates excellent reversibility and biocompatibility. Cysteine-containing copolymers have been explored to install free thiol groups onto the polymer chains, so the disulfide-crosslinked micelles can be generated under mildly oxidative conditions (11, 12). Alternatively, external disulfide-containing linkers may be used to produce the crosslinked micelles (13). Another elegant approach of introducing disulfide crosslinks has been recently demonstrated by Zhong *et al.*, where thioctic acid (TA), an endogenous metabolite and a naturally occurring antioxidant, is grafted onto the polymer backbone as a crosslinker (14, 15). The disulfide-containing thioctic ring is susceptible to ring-opening polymerization in the presence of a catalytic amount of dithiothreitol (DTT), which results in the formation of linear polydisulfide crosslinks between adjacent polymer chains within the micelles. The disulfide crosslinks are redox-responsive and prone to cleavage through thiol-disulfide exchange reactions with glutathione (GSH), an endogenous reducing agent present at much higher level in the cytosol of tissue cells (1–10 mM) than in plasma and the interstitial fluid (2–10 μM) (16). GSH level is found to be further elevated in the tumor cells (17), rendering disulfide-crosslinked micelles particularly suitable for intratumor delivery of anticancer drugs.

D-α-Tocopherol polyethylene glycol succinate 1000 ($TPGS_{1K}$) is an amphiphilic copolymer generated by coupling PEG 1000 ($PEG_{23}$) to Vitamin E succinate *via* an ester linkage. A safe pharmaceutical excipient approved by the FDA, $TPGS_{1K}$ has been extensively investigated as an emulsifier, solubilizer and stabilizer in a variety of nano-sized drug delivery systems such as nanoparticles and micelles (18). With high lipophilicity conferred by the aliphatic chain and aromatic ring of the Vitamin E moiety, the inclusion of $TPGS_{1K}$ in the mixed micelles not only greatly increases the loading capacity for hydrophobic drugs (19, 20), but also stabilizes the micellar core by reducing the molecular motion of the copolymers (20). Nevertheless, as a micelle forming copolymer itself, $TPGS_{1K}$ has an unfavorably high critical micelle concentration (CMC) at 0.2 g/L (18). By extending PEG to 2 kDa and conjugating it with VE at 1:2 molar ratio, the resulting $PEG_{46}$-$VE_2$ copolymer formed micelles at considerably lower CMC (1.14 mg/L), which could deliver doxorubicin with more potent anticancer efficacy than doxorubicin in the free form or in the $TPGS_{1K}$ micelles (21). In another recent study, it was demonstrated that by further increasing PEG size to 5 kDa, the $PEG_{114}$-$VE_2$ micelles (CMC≈1.8 mg/L) functioned as an improved formulation for paclitaxel and achieved stronger tumor

growth inhibition than Taxol® and paclitaxel-loaded $PEG_{46}$-$VE_2$ micelles (22).

In this study, we synthesized a novel copolymer comprised of PEG 5000 ($PEG_{114}$), VE and TA with a molar ratio of $PEG_{114}$:VE:TA at 1:4:4 (Fig. 1). The resulting $PEG_{114}$-$VE_4$-$TA_4$ copolymer could self assemble into micelles in aqueous solution with the CMC approximately 100 times lower than that of $TPGS_{1K}$. Catalyzed by trace amount of dithiothreitol (DTT), polydisulfide crosslinks were formed between the adjacent TA moieties within the micelles. The thermodynamic stability of the crosslinked $PEG_{114}$-$VE_4$-$TA_4$ micelles was markedly improved as reflected by a 10-fold decrease in the CMC than that of the non-crosslinked counterparts. Moreover, the crosslinked $PEG_{114}$-$VE_4$-$TA_4$ micelles remained intact in the presence of micelle-disrupting agents, signifying enhanced kinetic stability. While highly stable in the non-reducing environment, the crosslinked $PEG_{114}$-$VE_4$-$TA_4$ micelles were responsive to GSH at the intracellular level (10 mM), which accelerated drug release due to rapid de-crosslinking and disassembly of the micelles. Employing paclitaxel as a model hydrophobic drug, our study demonstrated that the crosslinked $PEG_{114}$-$VE_4$-$TA_4$ micelles improved the pharmacokinetic characteristics of paclitaxel in comparison with the non-crosslinked counterparts and Taxol®, leading to superior anticancer efficacy in mice bearing human ovarian cancer SKOV-3 xenografts.

## MATERIALS AND METHODS

### Materials

Monomethylterminated poly(ethylene glycol) monoamine, HCl salt ($CH_3O$-PEG-$NH_2$·HCl) with number average molecular weight (Mn) of 5,000 g/mol was purchased from Jenkem Technology (Beijing, China) and used without further purification. Nα-Fmoc-Nε-Boc-L-lysine (Fmoc-Lys(Boc)-OH), Nα,Nε-Fmoc-L-lysine (Fmoc-Lys(Fmoc)-OH) were purchased from P3Biosystems (Shelbyville, KY). N,N'-Diisopropylcarbodiimide (DIC), N-hydroxysuccinimide (NHS), ethyldiisopropylamine (DIEA), piperidine and trifluoroacetic acid (TFA) were obtained from Alfa Aesar (Ward Hill, MA). Vitamin E was purchased from Sigma (St. Louis, MO). 1-Hydroxybenzotriazole hydrate (HOBt) was purchased from AK Scientific Inc (Union City, CA). Paclitaxel was purchased from LC Laboratories (Woburn, MA). 1,10-Dioctadecyl-3,3,30,30-tetramethylindodicarbocyanine perchlorate (DiD) was purchased from Invitrogen (Grand Island, NY). 3,3'-Dioctadecyloxacarbocyanine, perchlorate (DiO) and 1,1'-dioctadecyl-3,3,3',3'-tetramethylindocarbocyanine perchlorate (DiI) were obtained from Biotium (Hayward, CA).

### Synthesis of the Copolymers

The $PEG_{114}$-$VE_4$-$TA_4$ copolymer was synthesized *via* stepwise peptide condensation reactions from MeO-PEG-$NH_2$·HCl. $PEG_{5K}$-$NH_2$ 1 (2 g, 0.4 mmol) was coupled by Fmoc-Lys(Boc)-OH (375 mg, 0.8 mmol) in the presence of DIC (150 μL, 0.96 mmol), HOBt (164 mg, 0.96 mmol) and DIEA (350 μL, 2 mmol) in DMF (50 mL) for 3 h at room temperature. The reaction mixture was poured into diethyl ether (200 mL) until the completion of the coupling reaction indicated by the Kaiser test. The precipitates were collected after centrifugation, washed by fresh ether (3×150 mL) and dried under vacuum to yield PEGylated compound 2. Fmoc groups were deprotected by the treatment with piperidine in DMF (*v*/*v* 1:4, 100 mL). The PEGylated compound were precipitated and washed with cold ether (200 mL). One more coupling of Fmoc-Lys(Boc)-OH and two more coupling of Fmoc-Lys(Fmoc)-OH were carried out step by step to furnish PEGylated compound 5. After the removal of Fmoc groups by piperidine in DMF, α-tocopheryloxyacetic acid synthesized according to a known method (23) was conjugated to the amino terminals of the lysines to afford PEGylated compound 6. The Boc groups of PEGylated compound 6 were removed by TFA in dichloromethane (*v*/*v* 1:3, 20 mL) for 30 min. The mixture was precipitated in cold ether and collected following centrifugation. Two coupling of Fmoc-Lys(Fmoc)-OH and one coupling of thioctic acid to the side amino groups of the PEGylated compound were further carried out according to the typical conjugation procedure. The $PEG_{114}$-$VE_4$-$TA_4$ copolymer was recovered from the mixture by repeated precipitation from DMF into diethyl ether. Finally, the copolymer was further purified by dialysis (3 kDa MWCO) against deionized water for 2 days and lyophilized to obtain an off-white solid. $^1$H-NMR spectra of the copolymers were collected at 20°C on a 600 MHz Agilent Inova Spectrometer (Santa Clara, CA) using $CDCl_3$ as a solvent.

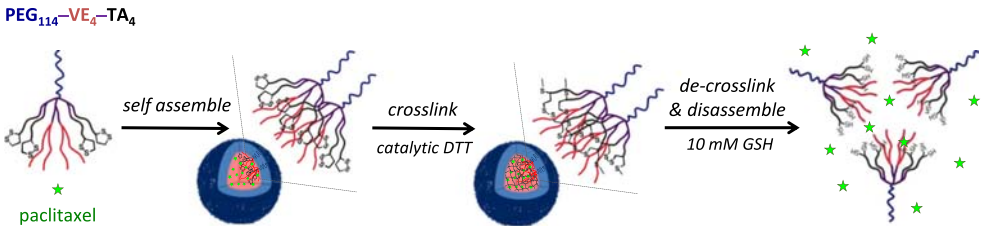


**Fig. 1** Schematic illustration of the design and action of the crosslinked $PEG_{114}$-$VE_4$-$TA_4$ micelles.

### Preparation of the Blank $PEG_{114}$-$VE_4$-$TA_4$ Micelles

The blank micelles were prepared by dissolving 90 mg $PEG_{114}$-$VE_4$-$TA_4$ copolymer in 1 mL phosphate buffered saline (PBS) following 20 min sonication. The micelle solution was divided equally into two portions, one of which remained unmodified to be the blank non-crosslinked micelles (B-NCMs). To the second portion, nitrogen gas ($N_2$) was bubbled for 10 min, and 10 μL of DTT (30 mg/mL in PBS) was then added to the micelle solution under a $N_2$ atmosphere, which was 5 mol% relative to the amount of thioctic units in $PEG_{114}$-$VE_4$-$TA_4$ polymer. The solution was shaken at 4°C for 24 h to form the blank crosslinked micelles (B-CMs). The UV absorbance of the micelle solution was measured at 330 nm to confirm the formation of the crosslinks among the TA moieties.

### Preparation of Paclitaxel-loaded $PEG_{114}$-$VE_4$-$TA_4$ Micelles and the NIR Dye-loaded $PEG_{114}$-$VE_4$-$TA_4$ Micelles

Drug-loaded micelles were prepare as reported previously (24). Briefly, the varying amount of paclitaxel and 90 mg $PEG_{114}$-$VE_4$-$TA_4$ were dissolved in 2 mL chloroform in a 25-mL round-bottom flask, which was rotor evaporated to dryness at room temperature to form a homogenous thin drug-copolymer film. The resulting thin film was further dried overnight under vacuum to remove any residual solvent. Paclitaxel-loaded non-crosslinked micelles (P-NCMs) were formed by hydrating the film in 1 mL PBS followed by 20 min sonication. To prepare the crosslinked micelles, $N_2$ was bubbled into 500 μL P-NCMs for 10 min, and 10 μL DTT (30 mg/mL in PBS) was then added to the micelle solution under a $N_2$ atmosphere. The solution was shaken at 4°C for 24 h to form paclitaxel-loaded crosslinked micelles (P-CMs). Following the crosslinking, the unreacted DTT was not removed, since the catalytic amount of DTT remaining in the micelle solution was well below the toxic levels when the cell culture and animal studies were carried out (25, 26). The loading concentration of paclitaxel in the micelles, defined as the amount of the drugs in the resulting micellar solution per unit volume of PBS, was quantified by HPLC as described below. The encapsulation efficiency of paclitaxel was calculated as the percentage of the incorporated *vs.* the input paclitaxel.

The near infrared (NIR) dye DiD and paclitaxel were co-loaded into the non-crosslinked (DP-NCMs) and crosslinked micelles (DP-CMs) using the same method as described above with the final DiD concentration as 0.1 mg/mL. DiO and DiI, a lipophilic fluorescence energy transfer (FRET) pair, were co-loaded into the crosslinked micelles using the same method with a final concentration of 0.25 mg/mL for each dye. All micelle formulations were filtered with 0.22 μm syringe filter for sterilization.

### Size and Zeta Potential of the $PEG_{114}$-$VE_4$-$TA_4$ Micelles

The hydrodynamic diameter and zeta potential of the micelles were recorded by dynamic light scattering (DLS) using a Nano Zetasizer ZS (Malvern Instruments, UK) equipped with He-Ne laser (4 mW, 633 nm) light source and 90° angle scattered light collection configuration.

### Transmission Electron Microscopy (TEM) of $PEG_{114}$-$VE_4$-$TA_4$ Micelles

The morphology of the micelles was observed at room temperature using a Tecnai G2 Spirit TEM (FEI, Hillsboro, OR). A drop of the micellar solution was deposited on a carbon-coated copper grid, dried at room temperature and negatively stained with 1% phosphotungstic acid before TEM visualization.

### CMC Determination of the $PEG_{114}$-$VE_4$-$TA_4$ Micelles

The CMC was determined by fluorescence spectra using pyrene as a fluorescent probe (27). Pyrene solution (20 μL, 0.5 mM in ethanol) was added into the glass tubes, and the solvent was evaporated at room temperature. B-NCMs or B-CMs solution was diluted in deionized water to the copolymer concentration ranging from 0.1 to 50 mg/L, which was added to the pyrene-containing glass tubes and gently shaken for 24 h to reach equilibrium before measurement. The fluorescence spectra of pyrene were recorded by a fluorescence spectrophotometer (Perkin Elmer, USA). The excitation wavelength at 331 nm and the emission fluorescence intensity at 373 nm and 393 nm values were used. The CMC was estimated from the threshold of the copolymer concentration, where the intensity ratio $I_{393}/I_{373}$ begins to increase markedly.

### Stability Studies of the $PEG_{114}$-$VE_4$-$TA_4$ Micelles

The storage stability of the $PEG_{114}$-$VE_4$-$TA_4$ micelles in PBS was assessed by monitoring the drug contents and the micelle size following incubation at 4°C for 4 weeks. To study the stability of the micelles in sodium dodecyl sulfate (SDS), P-NCMs or P-CMs were incubated with 2.5 mg/mL SDS solution at room temperature for 90 min. To evaluate the stability of the micelles in serum, the micelles were incubated in PBS containing 50% fetal bovine serum at 37°C for 24 h. The stability of P-CMs in PBS containing 2 μM or 10 mM GSH was studied at 37°C for 12 h. The size of the micelles was monitored by DLS. All samples were in triplicates.

### *In vitro* Release Study of Paclitaxel from the $PEG_{114}$-$VE_4$-$TA_4$ Micelles

The release of paclitaxel from the $PEG_{114}$-$VE_4$-$TA_4$ micelles was studied by a dialysis method. Paclitaxel-loaded micelles in

PBS was inserted into a Slide-A-Lyzer dialysis cassette (Thermo Scientific, Rockford, IL) with a 20 kDa MWCO. The cassette was submerged into 50 mL of PBS as the dialysis media at 37°C and swirled at 100 rpm. At predetermined time intervals, the sample was withdrawn from the cassette, the paclitaxel concentration was quantified by HPLC, and the dialysis media was refreshed to maintain the sink condition. To further investigate the release profile of the crosslinked micelles in response to reduction, the cassettes were also dialyzed against 50 mL PBS containing 2 μM or 10 mM GSH to mimic the extracellular and intracellular GSH level, respectively.

### Cell Culture

Human ovarian cancer SKOV-3 cells (American Type Culture Collection, Manassas, VA) were grown in DMEM medium (Invitrogen, Carlsbad, CA) with 2 mM L-glutamine, which was supplemented with 10% (*v*/*v*) fetal bovine serum, 100 units/mL penicillin G and 10 μg/mL streptomycin. The cells were maintained at 37°C with 5% $CO_2$ in a humidified incubator.

### Intracellular Uptake of the Crosslinked $PEG_{114}$-$VE_4$-$TA_4$ Micelles

To study the uptake of the crosslinked micelles, SKOV-3 cells were treated with DiI/DiO-dual loaded crosslinked micelles for 4, 6, 12 and 24 h. After removing the culture medium, cells were washed 3 times with cold PBS, and then trypsinized and re-suspended in PBS before being subjected to the flow cytometry analysis. Cell-associated fluorescence was analyzed using a BD Accuri C6 Flow Cytometer System (San Jose, CA). The fluorescence signals were acquired at the excitation wavelength of 488 nm. The spectral filters of $530 \pm 15$ nm and $585 \pm 20$ nm was used to detect DiO and DiI, respectively. All intensities were obtained with the same gain and offset. Data were analyzed using the FlowJo 9.3.1 software (Tree Star, Inc., Ashland, OR) and expressed as the geometric mean of the entire cell population.

### Cytotoxicity Assay

SKOV-3 cells were seeded at a density of 6,000 cells/well in 96-well plate, and treated in triplicates with various concentrations of blank micelles ($10^{-3}$–10 mg/L) or paclitaxel (1–100 nM) either in the free form, non-crosslink or cross-linked micelles for 72 h. Cells were then fixed with 1% glutaraldehyde, stained with 0.1% crystal violet, and dissolved in 10% acetic acid. The absorbance was quantified at 595 nm on FLUOstar Omega plate reader (Cary, NC). The relative cell viability was calculated as the percentage of absorbance of the treated *vs.* the untreated wells. Results are reported as the means for each triplicate samples.

### Tumor Xenograft Murine Model

All animal procedures were performed in strict accordance with the Guide for the Care and Use of Laboratory Animals of the National Institutes of Health. The protocol was approved by the Institutional Animal Care and Use Committee at Mercer University (Approval Number: A1105007). SKOV-3 cells ($2 \times 10^6$ in 0.1 mL matrigel/DMEM mixture) were subcutaneously implanted in each flank of 5–6 week-old female athymic nude mice (*nu/nu*, Charles River, Wilmington.)

### Pharmacokinetic Study

When the tumor volumes reached 100–300 $mm^3$, the mice were randomized into three treatment groups ($n=3$). Each group was i.v. administrated with Taxol®, P-NCMs and P-CMs at an identical dose of 5 mg/kg paclitaxel. The loading concentration of paclitaxel in both P-NCMs and P-CMs was 0.5 mM. At pre-determined time point, namely 5, 15, 30, 45, 60 and 90 min post administration, the blood samples were collected *via* retro-orbital bleeding. The concentration of paclitaxel in plasma was quantified by HPLC as described below. Non-compartmental analysis was performed to obtain the pharmacokinetic parameters including the elimination half-life ($t_{1/2,e}$), the total clearance ($CL_T$), and the apparent volume of distribution ($V_{d,ss}$) using the WinNonlin software (version 5.1, Pharsight, Sunnyvale, CA).

### HPLC Methodology

The Waters HPLC system (Milford, MA) consisted of a 2795 pump with an autosampler, a 996 photodiode array detector and a Phenomenex (Torrance, CA) $C_8$ column (5 μm, 4.6 mm × 150 mm). α-Naphthoflavone was used as an internal standard. The detection wavelengths for paclitaxel and α-naphthoflavone were 227 nm and 281 nm, respectively. An isocratic mobile phase of 28% (*v*/*v*) sodium phosphate buffer (25 mM, pH 3.0) with 10 mM triethylamine and 72% (*v*/*v*) methanol was used at a flow rate of 1.5 mL/min. The plasma samples were extracted by ethyl acetate, reduced to dryness under vacuum, and reconstituted with the HPLC mobile phase prior to HPLC analysis.

### *In vivo* NIR Imaging and Tissue Distribution

DiD, a lipophilic NIR dye (excitation: 644 nm, emission: 665 nm), was used to label paclitaxel-loaded $PEG_{114}$-$VE_4$-$TA_4$ micelles (11). DiD and paclitaxel were co-loaded into the micelles to form DP-NCMs and DP-CMs with a final paclitaxel concentration of 0.5 mM as previously described. When the tumor volume reached 100–300 $mm^3$, the mice were randomized into two treatment groups ($n=3$), and were i.v.

administrated with DP-NCMs or DP-CMs at a dose of 1.6 mg/kg DiD. At 0.083, 4, 8, 24 and 48 h post administration, the mice were anaesthetized by isoflurane and the whole-body images of the mice were scanned by Odyssey imaging system (LI-COR, Lincoln, NE). At 24 and 48 h, the mice were euthanized and the major organs including heart, liver, spleen, lung and kidney as well as the tumor tissues were excised and rinsed with PBS. The NIR signals were scanned and analyzed by Odyssey imaging system. The NIR intensity was quantified using the Odyssey Application Software (Version 3.021).

### Antitumor Efficacy Study

When the tumor volumes reached 50–100 $mm^3$, the mice were randomized into five treatment groups ($n=5$): (A) the untreated group; (B) the B-CMs group; (C) the Taxol® group; (D) the P-NCMs group; and (E) the P-CMs group. For Group B, the mice were i.v. administrated with an equal amount of the $PEG_{114}$-$VE_4$-$TA_4$ copolymer as Groups D and E. For Groups C, D, and E, the mice were i.v. administered with different paclitaxel formulations at 5 mg/kg twice-weekly for 3 weeks. The final concentration of paclitaxel in P-NCMs and P-CMs was 0.5 mM. The tumor size was measured using a caliper twice-weekly, and the tumor volume was calculated as $1/2 \times \text{length} \times \text{width}^2$. To monitor the overall toxicity, the body weight of all mice from the different groups was measured twice-weekly. The tumors were excised and divided for immediate formalin fixation and flash freezing (−80°C) for the histology/immunohistochemistry analysis and Western blotting.

### Histology and Immunohistochemistry

Formalin-fixed and paraffin-embedded tumor specimens of 3 to 4-μm thickness were sectioned and stained with hematoxylin and eosin (H&E) and the proliferating cell nuclear antigen (PCNA) antibody following the standard protocols.

### Western Blot Analysis

Tumor tissue samples (approximately 20–25 mg per sample) were homogenized and lysed using the RIPA buffer supplemented with the protease and phosphatase inhibitors. Tumor lysates containing 35 μg of total proteins were resolved onto 10% SDS-PAGE gels, and transferred onto the nitrocellulose membranes. Blots were probed with the antibodies for PCNA, phosphorylated Akt (p-Akt) and total Akt, all of which were from Cell Signaling (Danvers, MA). Anti-β-actin antibody (Santa Cruz Biotechnology, Santa Cruz, CA) was used as a loading control.

### Statistical Analysis

All data are presented as the mean ± standard deviation (SD). Data from the different groups were compared using the Student's *t*-test. A *p*-value of less than 0.05 was considered statistically significant, as indicated by asterisks in the figures.

## RESULTS AND DISCUSSION

### Synthesis and Characterization of the $PEG_{114}$-$VE_4$-$TA_4$ Copolymer

The synthesis of $PEG_{114}$-$VE_4$-$TA_4$ was shown in Scheme I. The completed reaction for each step was confirmed by the Kaiser test and thin layer chromatography. The structures of the $PEG_{114}$-$VE_4$-$TA_4$ copolymer and intermediates **5** and **6** were confirmed by $^1$H-NMR. As shown in Fig. 2a, the peaks for the aromatic hydrogen of the Fmoc group in compound 5 was observed at 7.2–7.8 ppm, with the characteristic peaks of the PEG chain ($-CH_2CH_2O-$) at 3.7 ppm and Boc hydrogen appearing at 1.3 ppm. The disappearance of the aromatic peaks and the presence of peaks for the alkyl hydrogen at 0.8–1.5 ppm indicate the complete de-protection of the Fmoc groups and the successful conjugation of VE in intermediate **6** (Fig. 2b). The thioctic acid (TA) structure could be observed from the peaks at 1.5–3.2 ppm in Fig. 2c. Moreover, $^1$H NMR showed that the alkyl peaks (0.8–1.4 ppm) and the phenymethyl peak (2.1 ppm) were not changed, indicating that the VE component remained intact during the Boc group de-protection by TFA. The average number of VE substituents per PEG chain could be determined by comparing the peak intensity of the terminal methyl group in VE (0.8 ppm) and the PEG methylene protons (3.70 ppm) in Fig. 2b. The average number of TA substituents per copolymer molecule could be also calculated by comparing the peak intensity at 2.2 ppm (α-methylene neighboring to the carbonyl group of TA) and 4.2 ppm (α-methylene neighboring to the carbonyl group of tocopheryloxyacetic acid) in Fig. 2c. The numbers of VE and TA units per PEG chain were 4.12 and 3.91, respectively, which were in good agreement with the molecular formula of the target copolymer. The final yield of $PEG_{114}$-$VE_4$-$TA_4$ copolymer was 78.3% relative to the starting material $PEG_{5K}$-$NH_2$.

### Preparation and Characterization of the $PEG_{114}$-$VE_4$-$TA_4$ Micelles

The crosslinking of the micelles was achieved by introducing DTT to the TA units in the micelles with a molar ratio of DTT:TA at 1:10 for 24 h. The UV spectra of the blank $PEG_{114}$-$VE_4$-$TA_4$ micelles in water showed that the


**Scheme I** Synthetic route of $PEG_{114}$-$VE_4$-$TA_4$. Reagents and condition: **a**, Fmoc-Lys(Bos)-OH, DIC, HOBt, DIEA, DMF, r.t, 6 h. **b**, i, 20% Piperidine in DMF, r.t, 2 h. ii, Fmoc-Lys(Bos)-OH, DIC, HOBt, DIEA, DMF, r.t, 6 h. **c** and **d**, i, 20% Piperidine in DMF, r.t, 2 h. ii, Fmoc-Lys(Fmoc)-OH, DIC, HOBt, DIEA, DMF, r.t, 6 h. **e**, i, 20% Piperidine in DMF, r.t, 2 h. ii, α-tocopheryloxyacetic acid, DIC, NHS, DIEA, DMF, r.t, overnight. **f**, i, 50% TFA in $CHCl_3$, r.t, 1 h. ii, Fmoc-Lys(Fmoc)-OH, DIC, HOBt, DIEA, DMF, r.t, 6 h. **g**, i, 20% Piperidine in DMF, r.t, 2 h. ii, lipoic acid, DIC, NHS, DMF, r.t, overnight

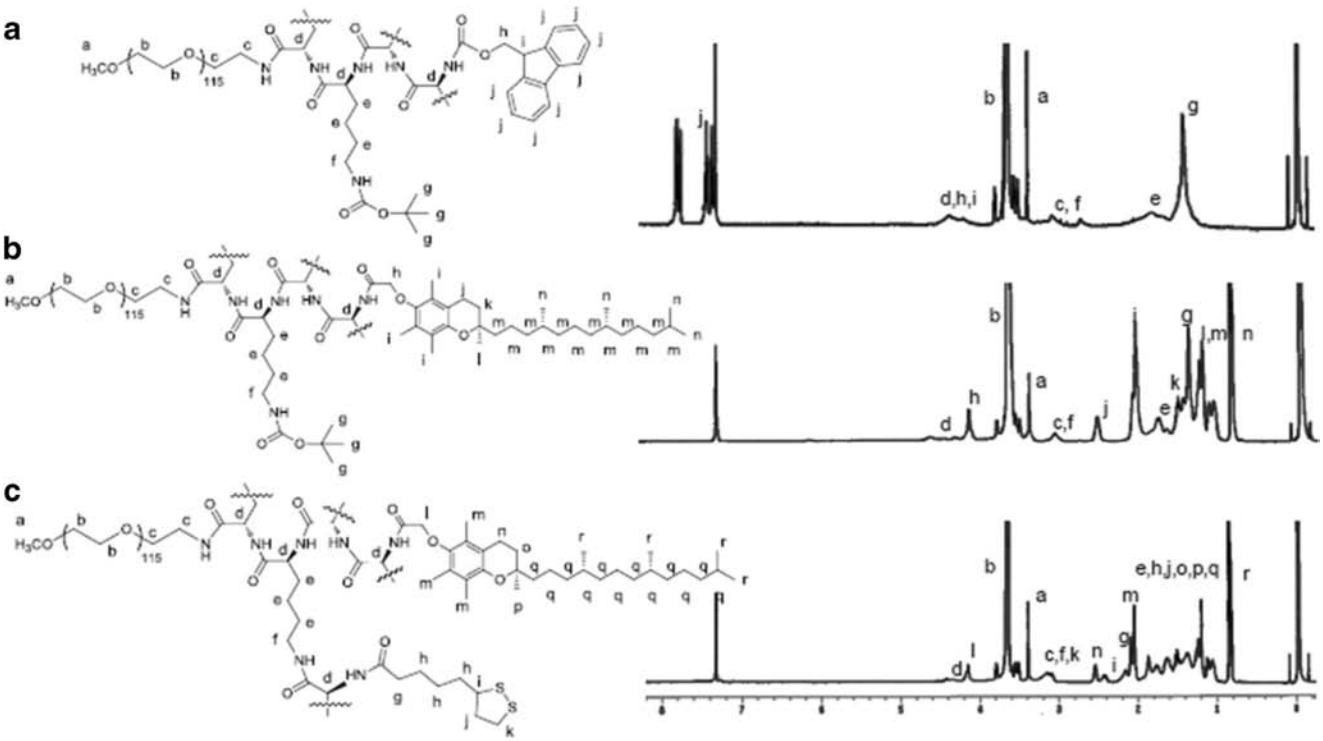


**Fig. 2** $^1H$ NMR spectra of intermediate **5** (**a**), **6** (**b**) and the $PEG_{114}$-$VE_4$-$TA_4$ copolymer (**c**) in $CDCl_3$.

absorbance of the disulfide-containing thioctic ring at 330 nm, which completely disappeared after crosslinking (Supplementary Material Fig. S1), indicating the breakage of the disulfide bond within the thioctic ring and the formation of linear polydisulfide bonds between adjacent TA units (28, 29). Paclitaxel-loaded $PEG_{114}$-$VE_4$-$TA_4$ micelles were further characterized with respect to their particle size and zeta potential (Table I and Fig. 3a–d). The average diameters of the crosslinked micelles (P-CMs) and their non-crosslinked counterparts (P-NCMs) were 43.9±2.6 nm and 45.4±2.5 nm, respectively. Their nearly identical sizes indicate that the cross-linkages among the TA moieties occur within the micelles, which has little influence on the hydrodynamic diameter of the micelles. The polydispersity indexes (PDI) of both formulations were less than 0.15, pointing to the narrow size distribution of the micelles and minimal inter-micellar aggregation during the crosslinking process. As expected, both micelle types had a close-to-neutral surface potential because of the uncharged $PEG_{114}$-$VE_4$-$TA_4$ copolymer. The spherical morphology and the size distribution of P-CMs and P-NCMs were confirmed by TEM (Fig. 3e, f).

To investigate the encapsulation capacity of the micelles for paclitaxel, $PEG_{114}$-$VE_4$-$TA_4$ copolymer at 10 mg/mL was used to encapsulate increasing input concentrations of paclitaxel, and the loading concentration and size distribution of the micelles were monitored. As shown in Table I and Supplementary Material S2A, the maximum loading of paclitaxel in P-NCMs and P-CMs was 4.72 mM and 4.33 mM, respectively, with the encapsulation efficiency of 94.4% and 86.8% when the input paclitaxel concentration was 5 mM. The CMC of the crosslinked $PEG_{114}$-$VE_4$-$TA_4$ micelles was 0.192 mg/L, which was over 10-fold lower than that of the non-crosslinked counterparts (2.26 mg/L). The pronounced decrease in the CMC of the crosslinked micelles provides strong evidence that the formation of polydisulfide crosslinks between adjacent $PEG_{114}$-$VE_4$-$TA_4$ copolymers within the hydrophobic region improves thermodynamic stability of the crosslinked micelles. The major advantages of the crosslinked $PEG_{114}$-$VE_4$-$TA_4$ micelles are two-folded: (1) the polysulfide crosslinks are formed readily and completely; (2) the hydrophobic payload can be stably incorporated into the micellar core with a high loading capacity.

### *In vitro* Stability of the $PEG_{114}$-$VE_4$-$TA_4$ Micelles

The storage stability of P-NCMs and P-CMs in PBS was evaluated by monitoring their size and paclitaxel loading (Fig. 4a). Both micelle types displayed excellent stability in PBS at 4°C for at least 4 weeks, reflected by little alteration in the particle size and less than 10% decrease in paclitaxel concentration in the micelle solution.

To investigate kinetic stability of paclitaxel-loaded $PEG_{114}$-$VE_4$-$TA_4$ micelles, we monitored the size of paclitaxel-loaded $PEG_{114}$-$VE_4$-$TA_4$ micelles in the presence of 2.5% sodium dodecyl sulfate (SDS), a strong surfactant that destabilizes supramolecular assemblies (30). SDS can form micelles itself in aqueous buffer with a particle size of less than 3 nm (31), which could aggregate with the $PEG_{114}$-$VE_4$-$TA_4$ unimers in the micellar solution, thus breaking the exchange equilibrium between the unimers and the $PEG_{114}$-$VE_4$-$TA_4$ micelles and eventually resulting in the disintegration of the micelle assemblies. As shown in Fig. 4b, in SDS-containing PBS the non-crosslinked micelles began to lose their initial size as early as 5 min, and almost completely disintegrated after 90-min incubation with the appearance of multiple particle peaks at different sizes. In contrast, the crosslinked micelles maintained their original size up to 90 min despite the presence of SDS.

When the micelles are administered intravenously, they first encounter the plasma proteins and the blood cells before reaching the target tissues, which may cause the destabilization of micelles and premature release of the payload. It is therefore crucial for the drug-loaded micelles to sustain the destabilizing environment in the bloodstream and remain associated during the circulation. To evaluate the stability of the micelles in serum, the particle size of micelles in 50% serum was monitored. As shown in Fig. 4c, the size of P-CMs was unaffected following 24 h-incubation in serum, while P-NCMs started to lose structural integrity within 2 h and formed larger aggregates at 24 h. Taken together, the above findings reveal that the crosslinked $PEG_{114}$-$VE_4$-$TA_4$ micelles possess improved kinetic stability. The polydisulfide crosslinks formed within the hydrophobic region of the micelles covalently link the $PEG_{114}$-$VE_4$-$TA_4$ copolymers and resist their dissociation from the micelle assemblies in the presence of micelle-disrupting agents.

**Table I** Characteristics of P-NCMs and P-CMs. Results show representative data obtained from at least three independent experiments and are reported as the mean ± SD ($n = 3$)

| Micelles | Size (nm)[a] | Zeta Potential (mV)[a] | PDI[a] | CMC (mg/l)[b] | Maximum Loading (mM)[c] |
|---|---|---|---|---|---|
| P-NCMs | 45.4±2.5 | 0.010±4.69 | 0.119±0.008 | 2.26±0.07 | 4.72±0.16 |
| P-CMs | 43.9±2.6 | −0.404±5.43 | 0.144±0.012 | 0.192±0.05 | 4.33±0.21 |

[a] Determined by DLS using Zetasizer Nano ZS at 25°C in DI water

[b] Determined using pyrene as a fluorescence probe

[c] Measured by HPLC with the polymer concentration at 10 mg/mL and the input paclitaxel concentration at 5 mM

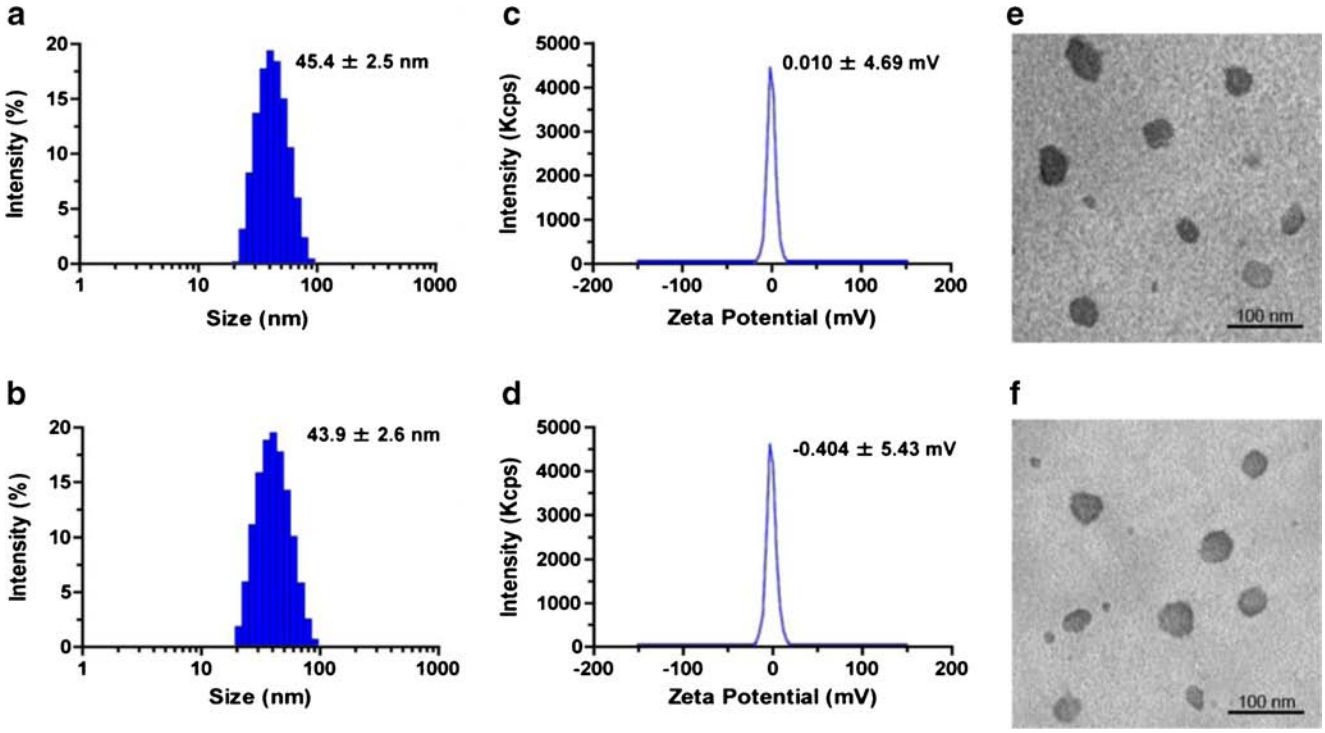


**Fig. 3** Size distribution and zeta potential of P-NCMs (**a** and **c**) and P-CMs (**b** and **d**). TEM images of P-NCMs (**e**) and P-CMs (**f**). Scale bars: 100 nm.

## De-crosslinking and Drug Release of the Crosslinked $PEG_{114}$-$VE_4$-$TA_4$ Micelles in Response to Reduction

It is known that the intracellular GSH level (1–10 mM) is much higher than the extracellular level (2–10 μM) (16). To study the reduction sensitivity of the crosslinked $PEG_{114}$-$VE_4$-$TA_4$ micelles, the change in the micelle size triggered by GSH at different time intervals was monitored (Fig. 5a). The particle size of P-CMs remained unchanged in PBS containing 2 μM glutathione during 12-h incubation, indicating excellent stability of the

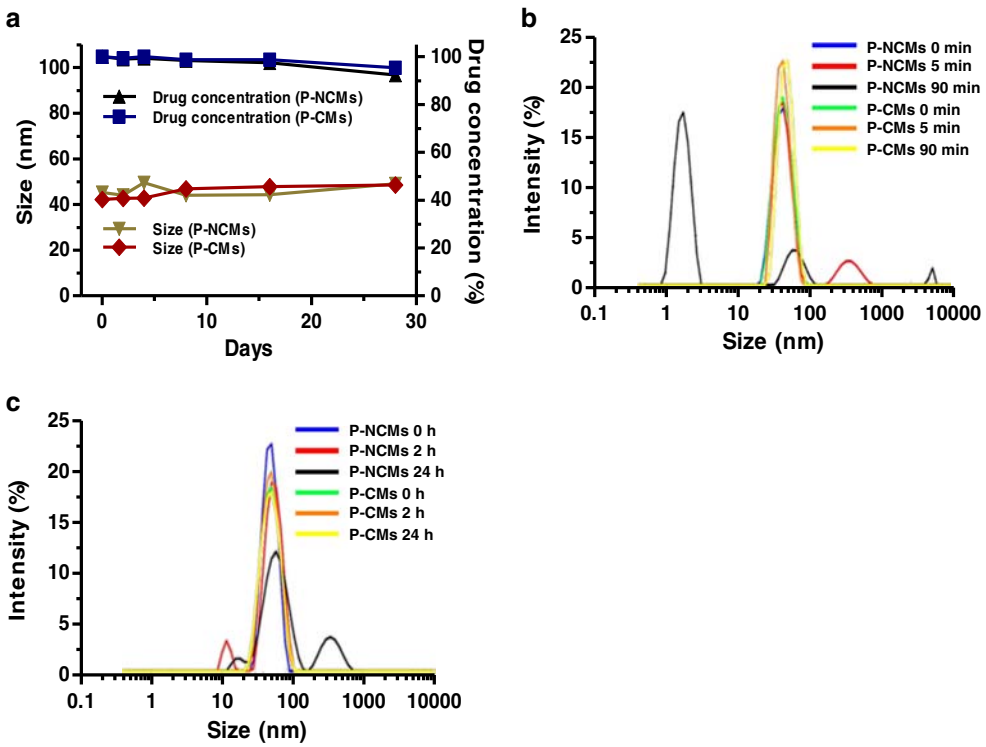


**Fig. 4** Stability of paclitaxel-loaded $PEG_{114}$-$VE_4$-$TA_4$ micelles. (**a**) The size and paclitaxel concentration of P-NCMs or P-CMs in PBS for 28 days. (**b**) The size distribution of P-NCMs and P-CMs in PBS containing 2.5 mg/mL SDS for 90 min. (**c**) The size distribution of P-NCMs and P-CMs in PBS containing 50% FBS for 24 h. All results show representative data obtained from at least three independent experiments.

crosslinked $PEG_{114}$-$VE_4$-$TA_4$ micelles in the non-reducing environment found in the bloodstream and tissue fluids. In contrast, multimodal peaks of larger aggregates appeared when the crosslinked micelles were incubated with 10 mM GSH for only 0.5 h. These results strongly suggest that the polydisulfide crosslinks within the P-CMs could be rapidly reduced and de-crosslinked by the intracellular level of GSH, leading to the disassembly of the micelles.

To evaluate the potential of the $PEG_{114}$-$VE_4$-$TA_4$ micelles as drug carriers, we studied the release kinetics of paclitaxel from the crosslinked $PEG_{114}$-$VE_4$-$TA_4$ micelles in comparison to the non-crosslinked counterparts. As shown in Fig. 5b, the release of paclitaxel from P-CMs was slow at the early time points, and there was less than 5% of drug release at 4 h, while P-NCMs lost 15.8% of the drug content over the same period. About 19.2% of paclitaxel was released from the P-CMs at 12 h, which was significantly lower than that released from P-NCMs (41.1%). It is expected that the crosslinking structure could not completely halt drug release from the micelles, however, these results support the notion that the polydisulfide crosslinks fortify the micellar structure and allow the crosslinked $PEG_{114}$-$VE_4$-$TA_4$ micelles to better retain the incorporated drug molecules within the micellar core.

To study the release of the drug-loaded crosslinked micelles in response to reduction, we performed the release study of P-CMs in PBS with the addition of 2 μM or 10 mM GSH, which corresponds to the extracellular and intracellular GSH levels, respectively. As shown in Fig. 5b, the presence of 2 μM GSH in the micellar solution did not alter the release profile of paclitaxel from P-CMs, pointing to excellent stability of the polydisulfide crosslinks in the non-reducing environment found in the circulation and tissue fluids. When GSH concentration was increased to 10 mM, 59.4% of the drug was released from P-CMs at 12 h, which was even faster than that of P-NCMs in the absence of GSH. The rapid release of P-CMs could be attributed to prompt breakdown of the disulfide linkages by GSH reduction. The resulting free thiols, highly hydrophilic groups, could drastically decrease the hydrophobic interactions inside the micellar core, leading to accelerated drug release. When the GSH concentration was between 2 and 50 μM, there was minimal destabilization of the crosslinked micelles; whereas a plateau of maximal destabilization was observed when the GSH concentration reached 1–10 mM (data not shown). These finding are also consistent with the above stability study (Fig. 5a) showing that P-CMs quickly lost structural integrity in PBS buffer containing 10 mM GSH. These results indicate that the crosslinking of micelles is reversible in the reducing environment prevalent in the cytoplasm of tissue cells.

## Intracellular Uptake of the Crosslinked $PEG_{114}$-$VE_4$-$TA_4$ Micelles

A fluorescence resonance energy transfer (FRET) pair of hydrophobic dyes, DiO (Ex/Em 488/501 nm) and DiI (Ex/Em 501/565 nm), was used to investigate the uptake of the crosslinked $PEG_{114}$-$VE_4$-$TA_4$ micelles into the tumor cells. FRET occurs when a donor dye (DiO) and an acceptor dye (DiI) are present within the range of Förster distance, the emission fluorescence from the excited donor dye is used as the excitation energy for the acceptor dye, resulting in the emission of the acceptor fluorescence (32). Since both DiO and DiI are encapsulated in the micellar core within Förster distance, when the micelles are exited at 488 nm, the emission energy from DiO can be transferred to adjacent DiI, which subsequently gets excited and emits the fluorescence at 565 nm. In contrast, when the micelles disintegrate or the dye molecules are released from the micelles, no fluorescence from DiI is emitted due to the lack of excitation energy. This feature could therefore be exploited to monitor the intracellular uptake of the intact micelles along with the entrapped payload.

The intracellular uptake of the crosslinked $PEG_{114}$-$VE_4$-$TA_4$ micelles was studied by directly determining the fluorescence signal of DiO/DiI-loaded micelles in human ovarian cancer SKOV-3 cells. As shown in Fig. 6a and Supplementary Material Fig. S4, when excited at 488 nm, the cells incubated with either DiO- or DiO/DiI-loaded micelles displayed strong green fluorescence signal at 530 ± 15 nm; whereas only the cells incubated with DiO/DiI-dual loaded micelles emitted red fluorescent signal at 585 ± 20 nm, no fluorescence signal was detected in the cells treated with DiI-loaded micelles. There was clear increase in

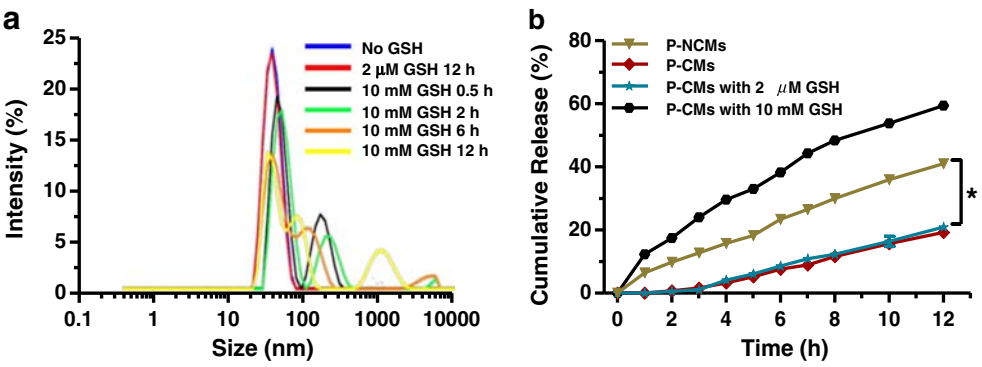


**Fig. 5** Reduction-responsiveness of P-CMs. (**a**) Stability of P-CMs in PBS containing 2 μM or 10 mM GSH for up to 12 h. (**b**) The release of paclitaxel from P-NCMs and P-CMs in the absence or presence of GSH. All results show representative data obtained from at least three independent experiments and are reported as the mean ± SD ($n = 3$). *, $P < 0.05$.

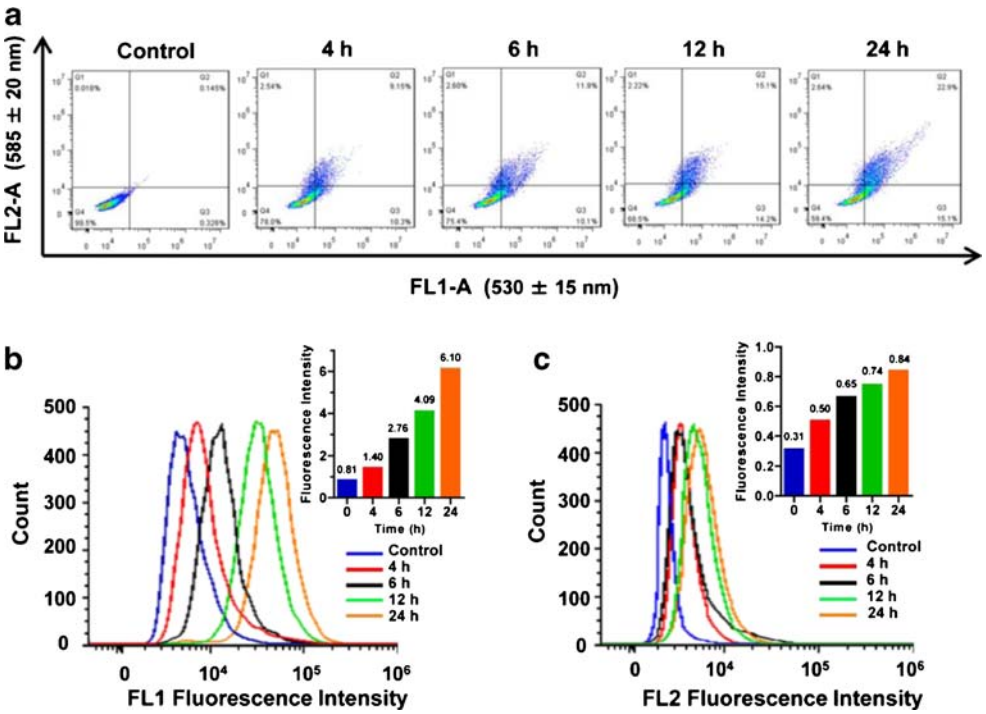


**Fig. 6** Intracellular uptake of the crosslinked $PEG_{114}$-$VE_4$-$TA_4$ micelles in SKOV-3 cells. Cells were incubated with DiO/DiI-dual loaded crosslinked micelles for up to 24 h. The intracellular fluorescence intensity was analyzed by a flow cytometer, as displayed in dot plots (**a**) and histogram plots (**b**, **c**). The inserts show the median fluorescence intensity (MFI) of each cell population. All results show representative data obtained from three independent experiments. The excitation wavelength was set at 488 nm, the FL1 channel had a spectral filter of 530 ± 15 nm to detect the fluorescence emission from DiO, and the FL2 channel with a spectral filter of 585 ± 20 nm to detect the fluorescence emission from DiI.

both green (FL1) and red fluorescence (FL2) over 24-h incubation period. Because the emission of red fluorescence by DiI requires excitation energy transferred from adjacent DiO, these results strongly suggested that the crosslinked $PEG_{114}$-$VE_4$-$TA_4$ micelles are internalized into the tumor cells with both dyes enclosed inside the micellar core. Similar results could be observed from the histogram analysis of the fluorescence intensity (Fig. 6b, c). Compared to the rising green fluorescence intensity emitted from DiO over time, the increase in the red fluorescence from DiI was less drastic. This could be explained by rapid decrosslinking of the micelles in the cytoplasm, resulting in less accumulation of DiI signal owing to the dissociation of the dye molecules from the micelles. Together, these results strongly imply that the crosslinked $PEG_{114}$-$VE_4$-$TA_4$ micelles can remain structurally intact and are taken up by the tumor cells along with the payload.

## Cytotoxicity of the Blank and Paclitaxel-loaded $PEG_{114}$-$VE_4$-$TA_4$ Micelles

To serve as a safe drug carrier system, it is desirable that the empty micelles are inert and devoid of cytotoxicity. Since all the building blocks in the $PEG_{114}$-$VE_4$-$TA_4$ copolymer are non-toxic in nature, the copolymer itself is expected to cause minimal cytotoxicity. To this end, we examined the cytotoxicity of the blank non-crosslinked (B-NCMs) and the blank crosslinked micelles (B-CMs) against SKOV-3 cells. We found that there was little cytotoxicity for both micelle types even at a

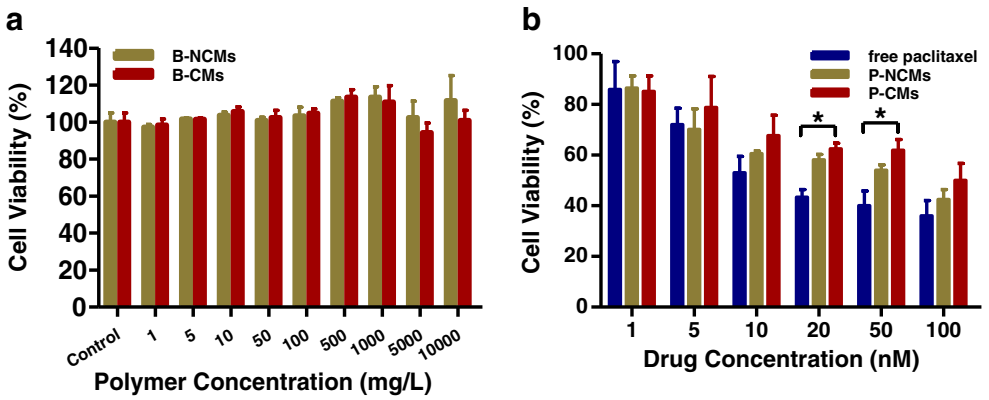


**Fig. 7** (**a**) Both the crosslinked and non-crosslinked $PEG_{114}$-$TA_4$-$VE_4$ micelles are minimally cytotoxic in SKOV-3 cells at the copolymer concentration up to 10 mg/mL. (**b**) The cytotoxicity of paclitaxel in the free form, or in the crosslinked or non-crosslinked $PEG_{114}$-$TA_4$-$VE_4$ micelles against SKOV-3 cells. Results show representative data obtained from at least three independent experiments and are reported as the mean ± SD ($n \geq 3$). *, $P < 0.05$.

polymer concentration up to 10 mg/mL (Fig. 7a), signifying the safety and biocompatibility of the $PEG_{114}$-$VE_4$-$TA_4$ copolymer.

Subsequently, the cytotoxicity of paclitaxel-loaded non-crosslinked (P-NCMs) and crosslinked micelles (P-CMs) was examined in SKOV-3 cells at paclitaxel concentration ranging from 1 to 100 nM for 72 h (Fig. 7b). Both micellar formulations displayed lower antiprolierative potency than free paclitaxel, which could be ascribed to the deterred drug release from the micelles. While the free drug could rapidly and passively diffuse into the tumor cells to exert the activity, the drug-loaded micelles could be only internalized into the cells *via* energy-dependent endocytosis, which is a slower and less efficient process than passive diffusion (33).

## Pharmacokinetics of Paclitaxel-loaded $PEG_{114}$-$VE_4$-$TA_4$ Micelles in Mice

In the clinic, paclitaxel is solubilized in Cremophor EL-based formulation (Taxol®) prior to intravenous administration. To evaluate the therapeutic utility of the crosslinked $PEG_{114}$-$VE_4$-$TA_4$ micelles as a nanocarrier system for the delivery of paclitaxel, we examined the pharmacokinetics of P-CMs, P-NCM and Taxol® at an identical dose of 5 mg/kg paclitaxel. As shown in Fig. 8 and Table II, the plasma concentration of paclitaxel from all three formulations declined in parallel with similar elimination half-lives ($t_{1/2,e}$), indicating identical elimination kinetics of paclitaxel regardless of the dosage forms. Importantly, intravenous administration of P-CMs resulted in approximately 5-fold and 3-fold higher paclitaxel level than those of Taxol® and P-NCM, respectively. Non-compartmental analysis on these profiles showed that compared to Taxol®, the incorporation of paclitaxel within the $PEG_{114}$-$VE_4$-$TA_4$ micelles reduced the volume of distribution ($V_{d,ss}$) of paclitaxel by 35% for P-NCMs and 76% for P-CMs. Consequently, the total clearance of P-NCM and P-CMs was 45% and 80% of Taxol®, respectively. Paclitaxel has a large

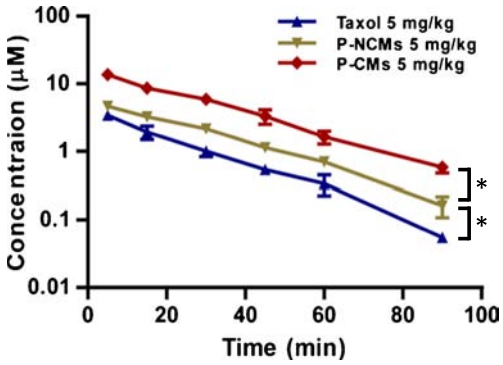


**Fig. 8** The plasma concentration of paclitaxel as a function of time following intravenous administration of Taxol®, P-NCMs and P-CMs at an identical dose of 5 mg/kg paclitaxel. Each data point represents the mean ± SD ($n = 3$). *, $P < 0.05$.

**Table II** Pharmacokinetic Parameters of Paclitaxel Following Intravenous Administration of Taxol®, P-NCMs and P-CMs in mice at an Identical dose of 5 mg/kg Paclitaxel. The results Represent the mean ± SD ($n = 3$)

| Parameters | Taxol® | P-NCMs | P-CMs |
|---|---|---|---|
| $t_{1/2,e}$ (min) | 14.2 ± 1.1 | 16.7 ± 0.7 | 17.2 ± 2.2 |
| AUC (μM·min) | 78.3 ± 9.5 | 139.6 ± 6.9 | 385.1 ± 33.5 |
| $CL_T$ (ml/kg/min) | 74.4 ± 8.4 | 40.8 ± 2.4 | 14.8 ± 1.2 |
| $V_{d,ss}$ (ml/kg) | 1521.6 ± 235.6 | 982.8 ± 12.8 | 366.8 ± 74.4 |

$V_{d,ss}$ because it is highly lipophilic and diffuses freely across the cell membrane throughout the body. When incorporated into the micelles, the distribution of the micellar paclitaxel became restricted largely within the vascular space due to the narrow fenestrations (<2 nm) in the epithelium of most healthy organs. It is inevitable, however, a fraction of the loaded paclitaxel would be released from the micelles during the circulation. The crosslinking of the micelles markedly decreased the release of paclitaxel and thus reduced its $V_{d,ss}$. These results clearly indicate that the $PEG_{114}$-$VE_4$-$TA_4$ micelles are able to retain paclitaxel within the micellar core and restrict the drug distribution into the extravascular space, whereas the crosslinking of the micelles further improves the drug retention within the micelles and prolongs the circulation time of paclitaxel.

## *In vivo* Biodistribution and Tumor Accumulation of DiD/Paclitaxel-Dual Loaded $PEG_{114}$-$VE_4$-$TA_4$ Micelles in Mice

To further investigate the pharmacokinetic characteristics of paclitaxel-loaded $PEG_{114}$-$VE_4$-$TA_4$ micelles, DiD, a hydrophobic NIR fluorescent dye which enables whole-body imaging with deep tissue penetration and low tissue absorption/scattering (34), was co-loaded with paclitaxel in the non-crosslinked (DP-NCMs) and the crosslinked (DP-CMs) micelles. We monitored the real-time *in vivo* biodistribution of DP-NCMs and DP-CMs by employing NIR imaging over 48 h. As a surrogate marker, the accumulation of DiD in the tumor reflected the extravasation of the micelles into the tumor *via* the EPR effect, a process begins immediately once the micelles enter the circulation and intensifies over the time. As shown in Fig. 9a, the NIR fluorescence signal was instantly detectable throughout the body following intravenous injection of both formulations because of rapid mixing of DP-NCMs and DP-CMs in the bloodstream. The contrast of the DiD signal in the tumors *vs.* the rest of the body became noticeable since 4 h post injection, suggesting that the preferential accumulation of the $PEG_{114}$-$VE_4$-$TA_4$ micelles in the tumor increased over time. The DiD intensity in the tumors treated with DP-CMs was higher than that of DP-NCMs, a clear indication of better tumor extravasation for

DP-CMs, which is consistent with improved kinetic stability of P-CMs in serum (Fig. 4c) and the prolonged circulation time of P-CMs *in vivo* as described above (Fig. 8). Notably, there was higher NIR fluorescent intensity in the chest area for the non-crosslinked micelles than that of the crosslinked micelles at 24–48 h, likely due to the more extensive distribution of free DiD released from DP-NCMs than that of DP-CMs, which is consistent with the pharmacokinetic analysis showing much reduced $V_{d,ss}$ of P-CMs compared to that of P-NCMs. As paclitaxel was quickly removed from the circulation (Fig. 8), the accumulation of paclitaxel in the tumor would occur to a much less extent than that of DiD following the micelle administration. Nevertheless, the trend of higher P-CMs accumulation in the tumor than P-NCMs should still hold true.

Next, the normal organs and tumor tissues were dissected for NIR imaging (Fig. 9b) and the fluorescence intensity was quantified (Fig. 9c). The DiD signal varied among the organs with the lowest found in the muscle and heart tissues for both formulations. There was a general trend that the DiD intensity in the well-perfused organs (liver, spleen, lung and kidney) decreased from 24 h to 48 h in DP-NCMs-treated mice, whereas the NIR signal remained same or slightly increased post DP-CMs injection. This may be rationalized by the fact that the crosslinked micelles remain intact in the circulation for a longer period of time than the non-crosslinking counterparts, resulting in more extended exposure of the payload in the well-perfused organs. Nevertheless, the difference in the NIR signal between the two micelle types in each corresponding normal organ was rather modest (<50% difference). By contrast, the NIR intensity of DP-CMs-treated tumors was 2.4-fold and 3.0-fold higher than that of non-crosslinked micelles at 24 h and 48 h, respectively. It is worth noting that the NIR intensity of the dissected organs did not completely agree with the whole-body imaging data. While the DiD imaging of the tumors appeared more prominent than any other organs in the body (Fig. 9a), the fluorescence intensity of the dissect tumors was actually similar to those of the liver (Fig. 9b). The discrepancy was caused by the varying distance of the organs away from the NIR scanning surface during the whole-body imaging study. Because the subcutaneous tumors were much closer to the scanning surface relative to the internal organs such as the liver, the fluorescence intensity of the tumors appeared much stronger than that of the liver even though both tissues had similar fluorophore levels. The NIR analysis of the dissected organs was performed when the organs were all laid on the same scanning surface, which was more accurate measurement of the tissue distribution than the whole body imaging. These findings strongly suggest that the crosslinking of $PEG_{114}$-$VE_4$-$TA_4$ micelles alters the biodistribution of the payload and preferentially enhances drug accumulation in the tumor *via* the EPR effect.

## Anticancer Efficacy of Paclitaxel-loaded $PEG_{114}$-$VE_4$-$TA_4$ Micelles in Tumor-bearing Mice

The major toxicities associated with Taxol® therapy include the hypersensitivity reactions caused by Cremophor EL and peripheral neuropathy induced by paclitaxel. It will be clinically beneficial to develop an alternative formulation for paclitaxel that: (1) requires no Cremophor EL as a solubilizer; (2) is amenable to more frequent and lower dosing to maximize the therapeutic window of paclitaxel. Encouraged by the

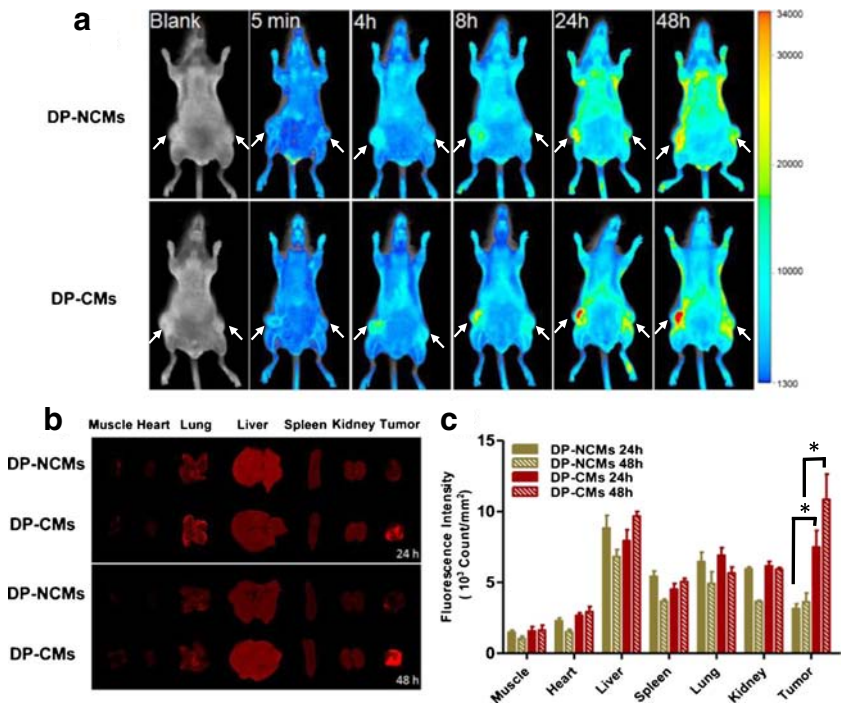


**Fig. 9** (**a**) Whole-body NIR imaging of SKOV-3 tumor-bearing mice treated with DiD/paclitaxel-loaded $PEG_{114}$-$VE_4$-$TA_4$ micelles for 48 h. DP-CMs and DP-NCMs were i.v. injected in mice at an identical dose with respect to DiD and paclitaxel. (**b**) NIR imaging of the normal organs and tumors excised at 24 h and 48 h post injection. (**c**) Quantitative measurement of the DiD intensity in the normal organs and tumors. Values are normalized by the scan area and reported as the mean + SD ($n = 3$). *, $P < 0.05$.

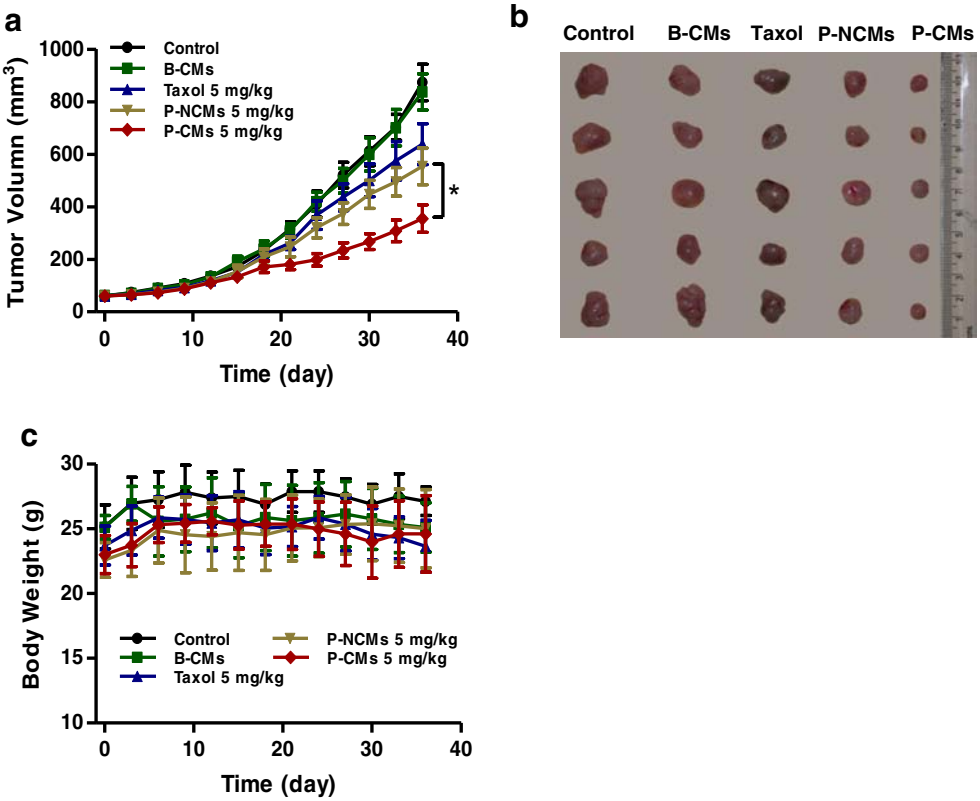


**Fig. 10** (**a**) Antitumor efficacy of paclitaxel-loaded $PEG_{114}$-$VE_4$-$TA_4$ micelles in mice bearing SKOV-3 tumors. P-NCMs, P-CMs and Taxol® were i.v. administered to the mice at 5 mg/kg paclitaxel twice-weekly for 3 weeks. B-CMs, P-NCMs and P-CMs were prepared with an identical polymer concentration. (**b**) Images of the tumors dissected from the tumor-bearing mice on day 35. (**c**) The average body weight of the mice in all groups. The results represent the mean ± SD ($n = 5$). *, $P < 0.05$.

promising pharmacokinetic results demonstrating that the encapsulation of paclitaxel within the $PEG_{114}$-$VE_4$-$TA_4$ micelles notably elevated the plasma concentration of paclitaxel and the crosslinking of the micelles further prolonged the circulation time of paclitaxel, we set out to evaluate the anticancer efficacy of paclitaxel-loaded $PEG_{114}$-$VE_4$-$TA_4$ micelles in tumor-bearing mice. Although Taxol® is found to be efficacious at a weekly dose of 20 mg/kg (35), we chose to treat the mice with twice-weekly 5 mg/kg paclitaxel to observe possible potentiation of its anticancer efficacy *via* the modified

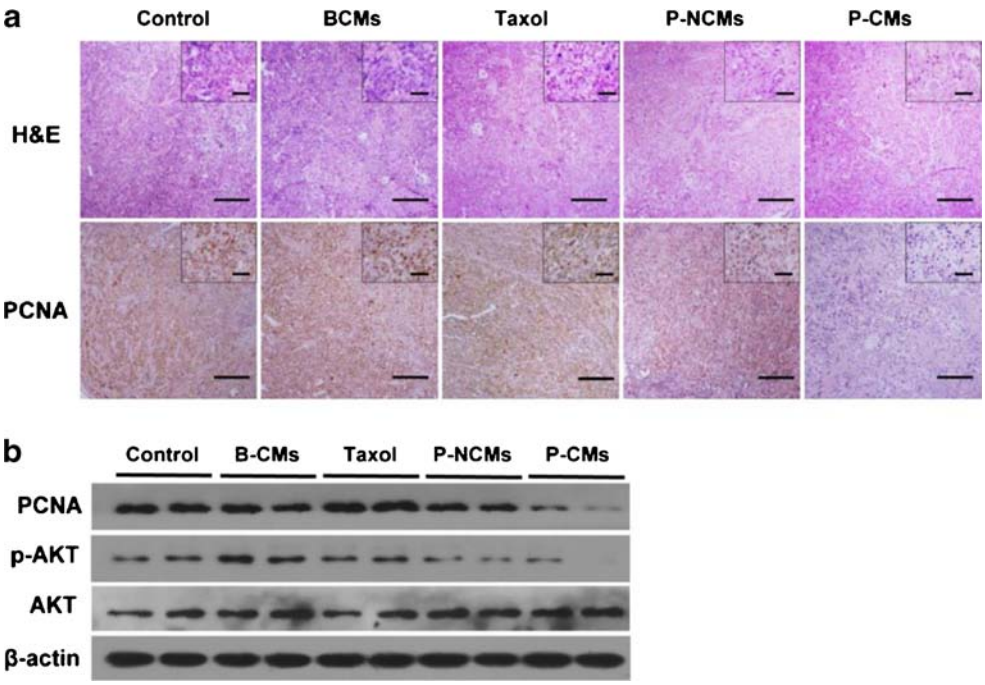


**Fig. 11** (**a**) H&E staining and immunohistochemistry staining for PCNA of the tumor sections. Scale bars: 200 μm in the large images and 100 μm in the small inserts. (**b**) The protein levels of PCNA and p-AKT in the tumor lysates by Western blot analysis. β-Actin was used as a loading control. All results show representative data of the tumor tissue samples.

formulations. As shown in Fig. 10a, b, SKOV-3 tumors in the untreated or B-CMs-treated groups grew rapidly over the 5-week study period, whereas Taxol® modestly slowed down the tumor growth compared with the untreated group ($p$=0.034 on 35th day) and P-NCMs exerted tumor growth inhibition similar to Taxol®. In contrast, P-CMs suppressed tumor growth with potency superior to P-NCMs and Taxol®, which became statistically significant starting day 24 ($p$<0.05). None of the treated mice experienced overt toxicity, as manifested by the steady body weight in all groups for 5 weeks (Fig. 10c).

To further confirm the therapeutic efficacy, *in vivo* antiproliferative effect of P-CMs and various formulations were examined by histological analysis of the tumors. H&E staining showed that the growth of the tumor was significantly inhibited by P-CMs with smaller cells and less nuclear division when compared with the rest groups (Fig. 11a). Immunohistochemistry staining with PCNA, a nuclear protein and a cell proliferation marker, demonstrated that the tumor cells in the P-CMs-treated mice underwent the least proliferation, whereas the high proliferation activity was observed in the tumors of the untreated, B-CMs and Taxol®-treated mice. This finding was further confirmed by Western blot analysis (Fig. 11b). In addition, p-Akt level was found to reduce markedly in the P-CMs-treated tumors, correlating well with the lower proliferative propensity of the tumor cells than that of the rest groups. Collectively, the above results provide strong evidence that the crosslinked $PEG_{114}$-$TA_4$-$VE_4$ micelles potentiate the anticancer efficacy of paclitaxel *in vivo*.

## CONCLUSIONS

In summary, we have synthesized redox-responsive $PEG_{114}$-$VE_4$-$TA_4$ copolymer, which could readily form micelles in aqueous solution and be further crosslinked by a catalytic amount of DTT. The crosslinked $PEG_{114}$-$TA_4$-$VE_4$ micelles demonstrated improved thermodynamic and kinetic stability, which significantly enhanced the delivery of paclitaxel to the tumor tissue and exert superior antitumor efficacy in a human ovarian cancer murine model. Constructing from all naturally occurring, biodegradable and/or biocompatible components, this novel crosslinked micellar nanocarrier system represents an interesting and promising platform for the delivery of sparsely aqueous soluble anticancer agents.

## ACKNOWLEDGMENTS AND DISCLOSURES

This work was supported by the National Institutes of Health grant R15 CA152860 to C.T.

Wei Fan and Yingzhe Wang contributed equally to the work.

## REFERENCES

1. Cheng Z, Zaki AAI, Hui JZ, Muzykantov VR, Tsourkas A. Multifunctional nanoparticles: cost versus benefit of adding targeting and imaging capabilities. Science. 2012;338(6109):903–10.
2. Kwon GS, Kataoka K. Block copolymer micelles as long-circulating drug vehicles. Adv Drug Deliv Rev. 2012;64:237–45.
3. Gong J, Chen M, Zheng Y, Wang S, Wang Y. Polymeric micelles drug delivery system in oncology. J Control Release. 2012;159(3):312–23.
4. Maeda H, Nakamura H, Fang J. The EPR effect for macromolecular drug delivery to solid tumors: improvement of tumor uptake, lowering of systemic toxicity, and distinct tumor imaging *in vivo*. Adv Drug Deliv Rev. 2013;65(1):71–9.
5. Owen SC, Chan DP, Shoichet MS. Polymeric micelle stability. Nano Today. 2012;7(1):53–65.
6. Chen H, Kim S, He W, Wang H, Low PS, Park K, *et al.* Fast release of lipophilic agents from circulating PEG-PDLLA micelles revealed by *in vivo* Förster resonance energy transfer imaging. Langmuir. 2008;24(10):5213–7.
7. O'Reilly RK, Hawker CJ, Wooley KL. Cross-linked block copolymer micelles: functional nanostructures of great potential and versatility. Chem Soc Rev. 2006;35(11):1068–83.
8. Read ES, Armes SP. Recent advances in shell cross-linked micelles. Chem Comm. 2007;29:3021–35.
9. van Nostrum CF. Covalently cross-linked amphiphilic block copolymer micelles. Soft Matter. 2011;7(7):3246–59.
10. Shao Y, Huang W, Shi C, Atkinson ST, Luo J. Reversibly crosslinked nanocarriers for on-demand drug delivery in cancer treatment. Ther Deliv. 2012;3(12):1409–27.
11. Li Y, Xiao K, Luo J, Xiao W, Lee JS, Gonik AM, *et al.* Well-defined, reversible disulfide cross-linked micelles for on-demand paclitaxel delivery. Biomaterials. 2011;32(27):6633–45.
12. Lee SY, Kim S, Tyler JY, Park K, Cheng JX. Blood-stable, tumor-adaptable disulfide bonded mPEG-$(Cys)_4$-PDLLA micelles for chemotherapy. Biomaterials. 2013;34(2):552–61.
13. Koo AN, Min KH, Lee HJ, Lee SU, Kim K, Kwon IC, *et al.* Tumor accumulation and antitumor efficacy of docetaxel-loaded core-shell-corona micelles with shell-specific redox-responsive cross-links. Biomaterials. 2012;33(5):1489–99.
14. Wei R, Cheng L, Zheng M, Cheng R, Meng F, Deng C, *et al.* Reduction-responsive disassemblable core-cross-linked micelles based on poly(ethylene glycol)-b-poly(N-2-hydroxypropyl methacrylamide)-lipoic acid conjugates for triggered intracellular anticancer drug release. Biomacromolecules. 2012;13(8):2429–38.
15. Wu L, Zou Y, Deng C, Cheng R, Meng F, Zhong Z. Intracellular release of doxorubicin from core-crosslinked polypeptide micelles triggered by both pH and reduction conditions. Biomaterials. 2013;34(21):5262–72.
16. Schafer FQ, Buettner GR. Redox environment of the cell as viewed through the redox state of the glutathione disulfide/glutathione couple. Free Radic Biol Med. 2001;30(11):1191–212.
17. Kuppusamy P, Li H, Ilangovan G, Cardounel AJ, Zweier JL, Yamada K, *et al.* Noninvasive imaging of tumor redox status and its modification by tissue glutathione levels. Cancer Res. 2002;62(1):307–12.
18. Zhang Z, Tan S, Feng SS. Vitamin E TPGS as a molecular biomaterial for drug delivery. Biomaterials. 2012;33(19):4889–906.
19. Mu L, Elbayoumi TA, Torchilin VP. Mixed micelles made of poly(-ethylene glycol)-phosphatidylethanolamine conjugate and D-α-tocopheryl polyethylene glycol 1000 succinate as pharmaceutical nanocarriers for camptothecin. Int J Pharm. 2005;306(1):142–9.
20. Chandran T, Katragadda U, Teng Q, Tan C. Design and evaluation of micellar nanocarriers for 17-allyamino-17-demethoxygeldanamycin (17-AAG). Int J Pharm. 2010;392(1):170–7.

21. Wang J, Sun J, Chen Q, Gao Y, Li L, Li H, *et al.* Star-shape copolymer of lysine-linked di-tocopherol polyethylene glycol 2000 succinate for doxorubicin delivery with reversal of multidrug resistance. Biomaterials. 2012;33(28):6877–88.
22. Lu J, Huang Y, Zhao W, Chen Y, Li J, Gao X, *et al.* Design and characterization of PEG-derivatized Vitamin E as a nanomicellar formulation for delivery of paclitaxel. Mol Pharm. 2013;10(8):2880–90.
23. Lawson KA, Anderson K, Menchaca M, Atkinson J, Sun L, Knight V, *et al.* Novel Vitamin E analogue decreases syngeneic mouse mammary tumor burden and reduces lung metastasis. Mol Cancer Ther. 2003;2(5):437–44.
24. Katragadda U, Fan W, Wang Y, Teng Q, Tan C. Combined delivery of paclitaxel and tanespimycin *via* micellar nanocarriers: pharmacokinetics, efficacy and metabolomic analysis. PLoS One. 2013;8(3):e58619.
25. Held KD, Melder DC. Toxicity of the sulfhydryl-containing radioprotector dithiothreitol. Radiat Res. 1987;112(3):544–54.
26. Carmack M, Kelley CJ, Harrison Jr SD. Optically active dithiothreitol. Toxicity and radiation-protective activity. J Med Chem. 1972;15(6):600–3.
27. Aguiar J, Carpena P, Molina-Bolivar JA, Ruiz CC. On the determination of the critical micelle concentration by the pyrene 1 : 3 ratio method. J Colloid Interface Sci. 2003;258(1):116–22.
28. Sadownik A, Stefely J, Regen SL. Polymerized liposomes formed under extremely mild conditions. J Am Chem Soc. 1986;108(24):7789–91.
29. Li YL, Zhu L, Liu Z, Cheng R, Meng F, Cui JH, *et al.* Reversibly stabilized multifunctional dextran nanoparticles efficiently deliver doxorubicin into the nuclei of cancer cells. Angew Chem Int Ed Engl. 2009;48(52):9914–8.
30. Kang N, Perron ME, Prud'homme RE, Zhang Y, Gaucher G, Leroux JC. Stereocomplex block copolymer micelles: core-shell nanostructures with enhanced stability. Nano Lett. 2005;5(2):315–9.
31. Bruce CD, Berkowitz ML, Perera L, Forbes MDE. Molecular dynamics simulation of sodium dodecyl sulfate micelle in water: micellar structural characteristics and counterion distribution. J Phys Chem B. 2002;106(15):3788–93.
32. Berney C, Danuser G. FRET or no FRET: a quantitative comparison. Biophys J. 2003;84(6):3992–4010.
33. Rejman J, Oberle V, Zuhorn IS, Hoekstra D. Size-dependent internalization of particles *via* the pathways of clathrin-and caveolae-mediated endocytosis. Biochem J. 2004;377(1):159–69.
34. Peng L, Liu RW, Marik J, Wang XB, Takada Y, Lam KS. Combinatorial chemistry identifies high-affinity peptidomimetics against α4β1 integrin for *in vivo* tumor imaging. Nat Chem Biol. 2006;2(7):381–9.
35. Kim SC, Kim DW, Shim YH, Bang JS, Oh HS, Kim SW, *et al. In vivo* evaluation of polymeric micellar paclitaxel formulation: toxicity and efficacy. J Control Release. 2001;72(1):191–202.